Synthesis, characterization and modeling of self-assembled porphyrin nanorods

Danielle Laurencin, Pascal Yot, Christel Gervais, Yannick Guari, Sébastien Clément, Erik Elkaim, Matthieu Paillet, Didier Cot, Sébastien Richeter

Synthesis, characterization and modeling of self-assembled porphyrin nanorods

Danielle Laurencin[a], Pascal G. Yot[a], Christel Gervais[b], Yannick Guari[a], Sébastien Clément[a], Erik Elkaim[c], Matthieu Paillet[d], Didier Cot[e], and Sébastien Richeter[a,*]

a Institut Charles Gerhardt de Montpellier, ICGM, UMR 5253, CNRS UM ENSCM, 34095 Montpellier, France

b Laboratoire de Chimie de la Matière Condensée de Paris, LCMCP, UMR 7574, Sorbonne Université, Collège de France, 75005 Paris, France

c Synchrotron SOLEIL, L'Orme des Merisiers Saint-Aubin, BP 48, 91192 Gif-sur-Yvette, France

d Laboratoire Charles Coulomb, L2C, UMR 5221, CNRS UM, 34095 Montpellier, France

e Institut Européen des Membranes, IEM, UMR 5635, Université Montpellier, ENSCM, CNRS, 34095 Montpellier, France

This paper is part of the 2019 Women in Porphyrin Science special issue

Received date (to be automatically inserted after your manuscript is submitted)
Accepted date (to be automatically inserted after your manuscript is accepted)

ABSTRACT: Porphyrin nanorods were prepared by ion-association between free base m*eso* 5,10,15,20-tetrakis-(4-*N*-methylpyridinium)porphyrin cations and tetraphenylborate anions. The nanorods had variable length (up to a few micrometers long) and diameters (~50-500 nm). Their structure at the molecular level was elucidated by combining multinuclear solid state NMR spectroscopy, synchrotron X-ray powder diffraction and DFT calculations.

KEYWORDS: porphyrin, nanorods, self-assembly, solid state NMR, NMR cristallography, DFT modeling

*Correspondence to: Sébastien Richeter, Institut Charles Gerhardt Montpellier, ICGM, UMR 5253, CNRS, Université de Montpellier, ENSCM, Place Eugène Bataillon, 34095 Montpellier cedex 5 (France). E-mail : sebastien.richeter@umontpellier.fr. Tel. : ++(33)467143971.

INTRODUCTION

Natural photosynthetic light-harvesting systems such as chlorosomes of green photosynthetic bacteria play key roles such as photon capture and energy transfer. Chlorosomes of green photosynthetic bacteria are very efficient natural light harvesting complexes [1]. They contain on the order of 10^5 bacteriochlorophyl molecules which are organized into rod-shaped aggregates [2]. Porphyrins are attractive compounds for the design of materials having advanced properties such as photonic wires [3], nonlinear optical materials [4], photovoltaic cells [5] or artificial photosynthetic reaction centres [6]. To avoid complicated multi-step synthetic procedures to obtain multiporphyrinic systems [7], molecular self-assembly processes are attractive for preparing porphyrin nanoparticles [8,9], nanorods [10,11], nanofibers [12], nanotubes [13], and other nanostructures with different morphologies [14].

The self-organization of porphyrin derivatives into nanoscale superstructures is generally driven by non-covalent interactions such as van der Waals forces, hydrogen bonding, π–π interactions, ionic interactions and/or coordinative binding [14]. Investigation of the morphology of these nanostructures is usually performed using imaging techniques like transmission electronic microscopy (TEM), scanning electronic microscopy (SEM) or atomic force microscopy (AFM) [8-14]. UV-visible absorption spectroscopy can also be helpful to determine if porphyrins self-assemble to form *J*- or *H*-aggregates: the Soret absorption is generally redshifted upon formation of *J*-aggregates, while it is blueshifted upon formation of *H*-aggregates [15]. If sufficiently crystalline materials are obtained, X-ray powder diffraction (XRPD) data can also be used to determine space group, unit cell dimensions and some important structural parameters like interplanar distances, which may also be observed by HR-TEM (High Resolution TEM) [16,17]. According to the obtained data, models can be proposed to show how porphyrins and other molecular species are assembled [18]. Moreover, multinuclear solid state NMR has been used in a small number of cases [19].

In this manuscript, we present the synthesis and full characterization of self-assembled porphyrin based nanorods made of free base m*eso* 5,10,15,20-tetrakis-(4-*N*-methylpyridinium)porphyrin cations (**TMPyP^{4+}**) and tetraphenylborate anions (**BPh$_4^-$**) (Chart 1). These two building blocks were previously used for the synthesis of porphyrin nanoparticles without self-aggregation [20,21]. Here, it will be shown how detailed information on the mode of association of these building blocks at the nanoscale can only be reached by combining a wide diversity of analytical techniques (including synchrotron powder X-ray diffraction and multinuclear solid state NMR) to *ab intio* DFT calculations. The characterization strategy described herein should therefore be of interest to the study of a variety of other porphyrin nanostructures.

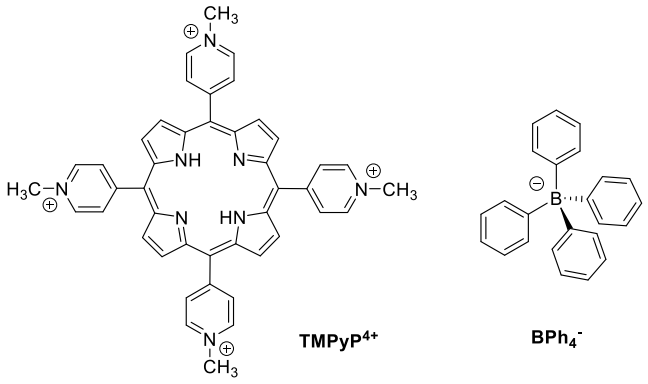

Chart 1. Structures of the **TMPyP^{4+}** and **BPh$_4^-$** building blocks for the synthesis of porphyrin nanorods.

RESULTS AND DISCUSSION

Synthesis and morphology of porphyrin nanorods.

M*eso*-5,10,15,20-tetrakis-(4-*N*-methylpyridinium) porphyrin (**TMPyP^{4+}**) is a water-soluble cationic porphyrin, which has been actively used as a water-soluble porphyrin derivative for various biomedical applications, where it can play the role of a photosensitizer for photodynamic therapy (PDT) applications [22,23] or as ligand able to bind DNA structures like G-quadruplexes [24-27]. **TMPyP^{4+}** has also been used as a cationic building block to obtain self-assembled nanostructures. For example, Yao *et al*. showed that **TMPyP^{4+}** can self-assemble with tetraphenylborate (**BPh$_4^-$**) in water to form spherical organic nanoparticles with an average diameter of 25±3 nm [20,21]. These ion-pair-based nanoparticles could be sterically stabilized with polyvinylpyrrolidone (PVP). Here, by avoiding the use of PVP and using slightly different reactions conditions, we were able able to synthesize porphyrin based nanorods using these same ions.

In our synthetic approach, the solvent system we used for the preparation of nanorods was a 3:1 (*v*:*v*) EtOH/H_2O mixture, and the final concentrations of the **TMPyP^{4+}** and **BPh$_4^-$** ions in the reaction mixture were fixed at 0.03 and 0.12 mM, respectively (*i.e.* four equivalents of tetraphenylborate anions compared to the porphyrin). Reactions were performed during 24 hours at 15°C and 30°C. Upon mixing **TMPyPI$_4$** with **NaBPh$_4$**, an immediate change in color from purple to orange occurred as a consequence of the aggregation of the two building blocks. However, no immediate precipitation was observed thanks to the presence of EtOH, allowing UV-visible absorption spectroscopy analyses to be performed in the early stage of the reaction (10 minutes after mixing **TMPyPI$_4$** with **NaBPh$_4$**). The spectra obtained confirmed that aggregated species are formed since the Soret absorption band of **TMPyP^{4+}** in the reaction mixture was broader and bathochromically shifted compared to the Soret absorption band of **TMPyP^{4+}** alone in H_2O (Figure 1a). The four Q bands also appeared to be bathochromically shifted. This spectral evolution could be in agreement with a flattening of the porphyrin and a larger π conjugation between the porphyrin core and the *meso* pyridinium groups (*vide infra*, X-ray powder diffraction analysis and DFT calculations). After 24 hours at 15°C, a mixture of nanofibers with nanoparticles stuck onto them was observed by TEM. When the same reaction was performed at 30°C, nanorods of variable length (up to a few micrometers long) and diameter (~50-500 nm) were formed. These nanorods could be rather well dispersed according to TEM and AFM (Figures 1b and 1d), but tended to form bundles upon removing the solvent mixture, as it can be seen by SEM (Figure 1c). A few milligrams of brown nanorods could be isolated in the solid state, which were then studied by solid state NMR and XRD.

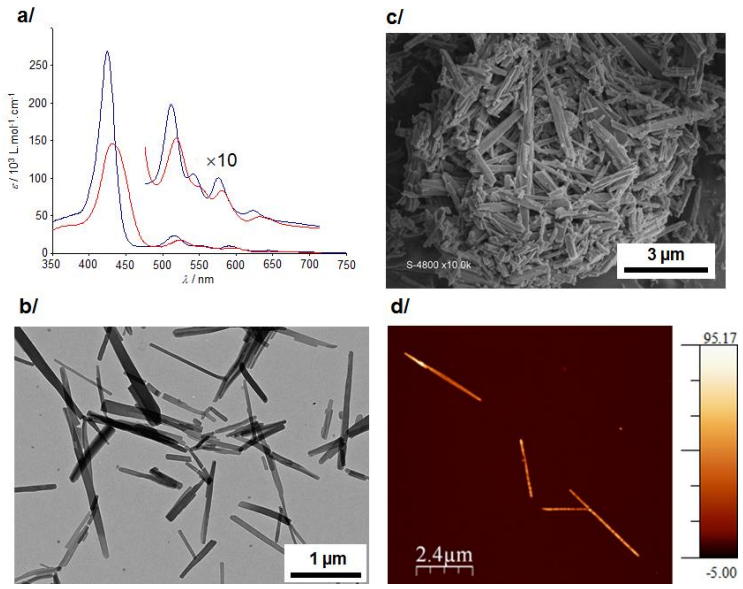

Fig. 1. a/ UV-visible absorption spectra of the **TMPyP^{4+}** precursor (blue) and of the reaction mixture after 10 minutes of reaction (red) in EtOH/H_2O 3:1. b/ TEM, c/ SEM and d/ AFM images of the nanorods.

Solid state NMR analyses

Multinuclear MAS (magic angle spinning) solid state NMR analyses were carried out on the isolated nanorods, in view of bringing direct evidence that these are formed by association of **TMPyP^{4+}** and **BPh$_4^-$** ions (Figure 2). First, it is clear that NMR signatures characteristic of both **TMPyP^{4+}** and **BPh$_4^-$** building-blocks can be observed on the ^{1}H, ^{13}C and/or ^{11}B solid state NMR spectra of the nanorods. For example, the ^{1}H resonance centered at ~ -3 ppm is characteristic of the internal N<u>H</u> of the porphyrin, the ^{13}C resonance centered at 43 ppm belongs to the methyl group of the *meso* 4-N-methylpyridyl moiety of the porphyrin, while the ^{11}B resonance observed by ^{11}B NMR can only be assigned to tetraphenylborate anions. Second, it is also clear from the ^{1}H, ^{13}C and ^{11}B MAS NMR spectra that the local environments of the **TMPyP^{4+}** and **BPh$_4^-$** building blocks within the nanorods differ from those of the starting reagents. For instance, when considering the characteristic resonances mentioned previously, the ^{1}H resonance of the porphyrin N<u>H</u> is deshielded in the nanorods, the ^{13}C resonance of the methyl group in the *meso* 4-N-methylpyridyl moiety is more shielded than in the porphyrin precursor, and the ^{11}B signal of the tetraphenylborate ions is much broader in the nanorods than in the Na salt used in the reaction.

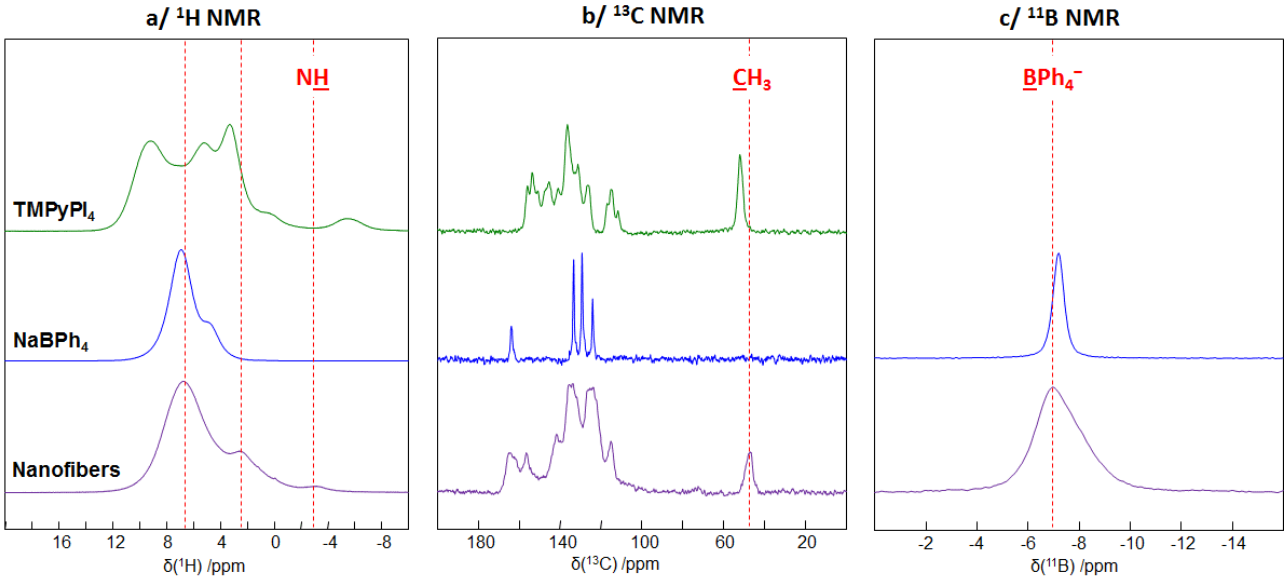

Fig. 2. Solid state NMR spectra of **TMPyPI$_4$** (green), **NaBPh$_4$** (blue) and the porphyrin nanorods (purple) recorded at 14.1 T under MAS, for (a) ^{1}H, (b) ^{13}C and (c) ^{11}B. Details on the acquisition conditions can be found in the experimental section.

Using two-dimensional ^{1}H-^{11}B correlation experiments, in which the "through-space" proximity between ^{1}H and ^{11}B nuclei is probed (through the dipolar coupling interaction), complementary informations on the association between **TMPyP^{4+}** and **BPh$_4^-$** ions was obtained. Indeed, as shown on the CPMAS (cross polarization magic angle spinning) NMR spectra in Figure 3, an interesting cross-peak is first observed for a contact time (CT) of 4 ms, between the ^{11}B resonance of the **BPh$_4^-$** ion and a ^{1}H resonance centered at ~ 2 ppm (orange circle). Given that this ^{1}H resonance belongs tothe protons of the porphyrin C<u>H</u>$_3$ group (see Figure S1, supporting information), such analyses confirm the spatial proximity of the two ions within the nanorods. When increasing the contact time to 8 ms, an additional cross-peak is observed, correlating the ^{11}B resonance of the **BPh$_4^-$** ion and a ^{1}H resonance centered at ~ -3 ppm, which

belongs to the NH of the porphyrin (green circle). The need for longer contact times to observe this cross-peak suggests that within the nanofibers, both ions are associated in such a way that the B atoms are closer to the CH_3 protons than the NH.

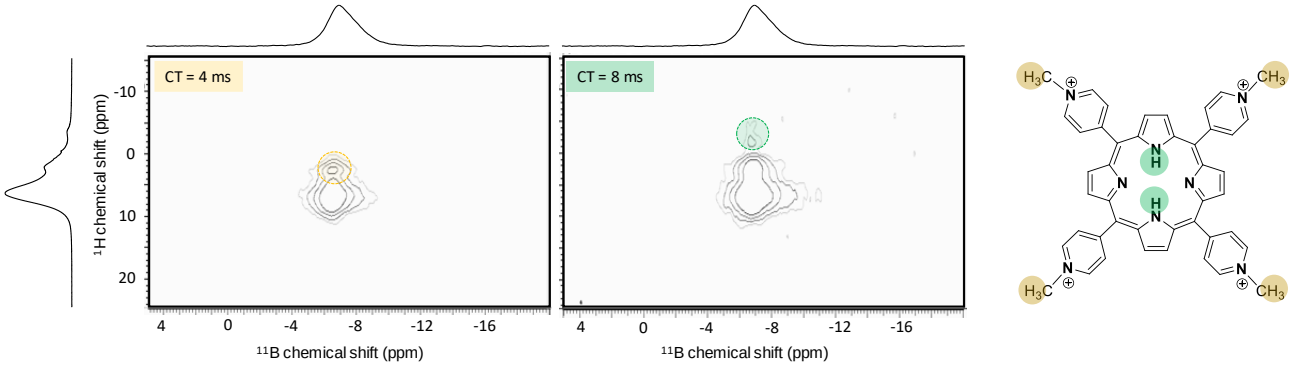

Fig. 3. ^{1}H-^{11}B CPMAS NMR spectra of the porphyrin nanofibers recorded at 14.1 T under MAS, using contact times (CT) of 4 ms (left) and 8 ms (right). The cross-peak highlighted in orange at CT = 4 ms attests of a close proximity between the boron of **BPh_4^-** and methyl group of the porphyrin, while the cross-peak highlighted in green at CT= 8 ms shows that the NH of the porphyrin is more distant from the **BPh_4^-** anion. The projections shown along both axes correspond to the 1D ^{1}H and ^{11}B MAS NMR spectra.

X-ray powder diffraction analysis and DFT modeling

In order to go further into the structural analysis of the nanorods, and to provide deeper insight into the mode of association of the cationic and anionic building blocks at the molecular level, high-resolution synchrotron X-ray powder diffraction (S-XRPD) analyses and computational modeling were used. It should be noted that due to the "nano" nature of these particles, and their tendency to aggregate in the dry state, no crystals of sufficient size and quality could be isolated for single-crystal X-ray diffraction studies. Here, the S-XRPD data were collected at 125 K and at room temperature at the Soleil synchrotron (Gif-sur-Yvette, France) on the CRISTAL beamline, and the powder patterns were examined using the FoX (Free Objects for Crystallography) software, in order to determine the unit cell parameters. Results for the two considered temperatures are represented in Figures 4a (below) and S2 (Supporting Information), and the full unit cell parameters at both temperatures are provided in Table S1 (Supporting Information).

For the data obtained at 125K, a preliminary structural model was derived from the powder pattern using FoX, considering a **$TMPyP^{4+}$/BPh_4^-** molar ratio of 1:4, as had been used during the synthesis. This model was then optimized using DFT, by relaxing all atomic positions but keeping cell parameters fixed to the experimental values. It should be noted that relaxation of all atomic positions (and not H positions only) was found to be critical at this step to achieve a suitable geometry for the two building blocks, and also to obtain a better agreement between experimental and DFT-calculated NMR parameters. This is demonstrated in Fig. 4b, in which the experimental ^{13}C CPMAS spectrum of the nanorods is compared to the calculated ^{13}C shifts for two structural models, obtained after relation of all atomic positions or of H atoms only. A better agreement is obtained in the former case, and this is also true when performing similar analyses of the experimental *vs* calculated ^{11}B NMR data (Tables S2 and S3 in the Supporting Information).

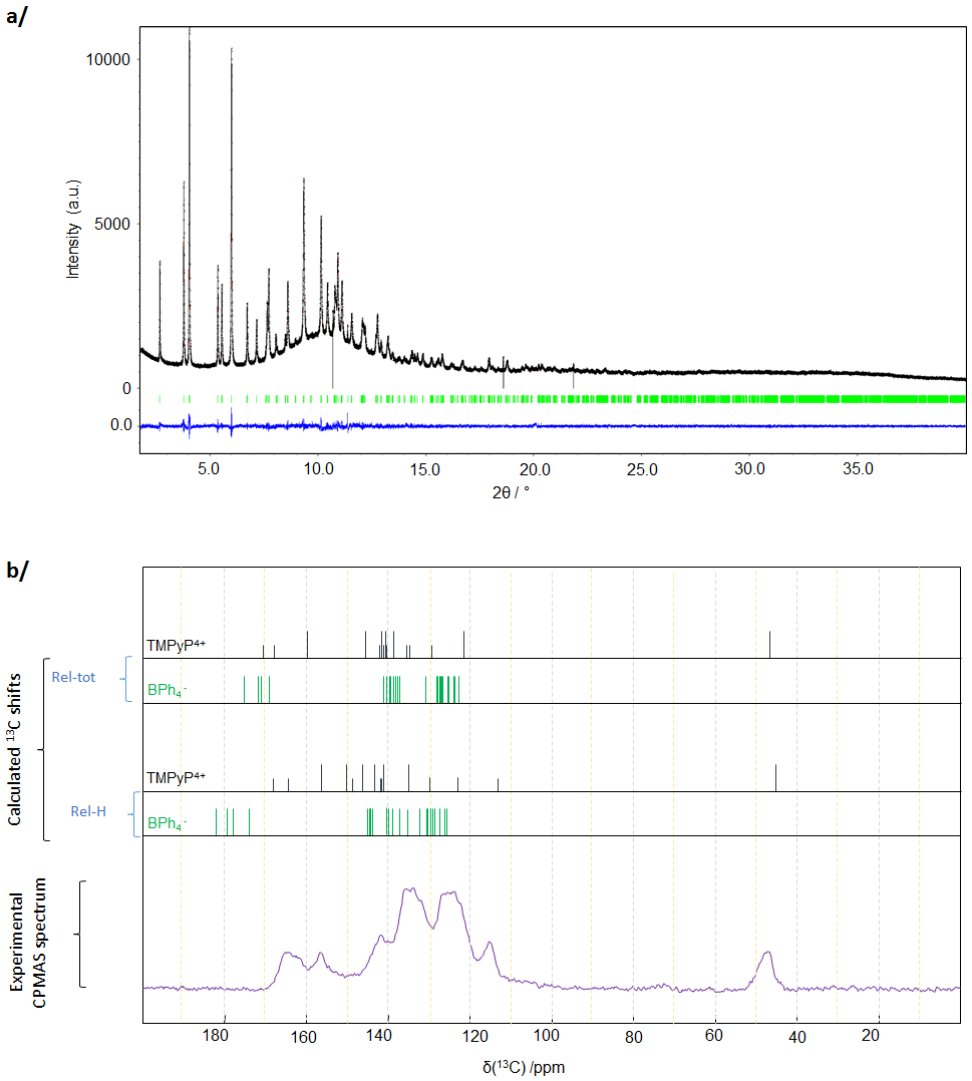

Fig. 4. a/ Structure-independent refinement of the unit-cell of the diffraction pattern obtained for the nanorods at 125 K. Observed (black line) and calculated (red line mostly hidden by the black line) X-ray powder diffraction profile for the LeBail refinement. The bottom curve (blue line) is the difference plot on the same scale intensity and the tic marks (in green) are the calculated angles for the Bragg peaks in 2θ. b/ Comparison of experimental ^{1}H-^{13}C CPMAS NMR spectrum of the nanorods with the ^{13}C chemical shifts calculated by DFT, for models in which either H positions or all atomic positions were relaxed. It should be noted that for reasons of clarity of the figure, the ^{13}C resonances reported here (as verticle bars) were derived from the values found in Tables S2 and S3, by averaging the ^{13}C shifts of positions corresponding to chemically equivalent carbon atoms.

The structural model of the nanorods, derived from this multi-technique approach combining S-XRPD, multinuclear solid state NMR and DFT calculations, sheds light on the self-assembly process which takes place during the synthesis. The obtained asymmetric unit and the packing mode of **TMPyP^{4+}** and **BPh$_4^-$** are represented in Figures 5a to 5c. As illustrated in Figure 5a, **TMPyP^{4+}** self-assemble with **BPh$_4^-$** to form columns of **TMPyP^{4+}** along the *c* crystallographic axis. The mean planes (based on least-square planes calculated for the 24 core atoms of the porphyrin core) of two successive porphyrins within these columns are separated by ~11.6 Å indicating that there is no π-overlap between them. As a consequence, the bathochromic shift of the absorption bands observed by UV-visible absorption spectroscopy (Fig. 1a) is not due to the aggregation of **TMPyP^{4+}**, but may be attributed to the flattening of the porphyrin and the larger π conjugation between the macrocycle and the *meso* pyridinium groups. In the absence of **BPh$_4^-$**, pyridinium groups are nearly perpendicular to the mean plane of the porphyrin core [28]. In the presence of **BPh$_4^-$** within the nanorods, the four dihedral angles between the pyridinium groups and the mean plane of porphyrin

core are ~31.5°, ~56.0°, ~62.3° and ~63.7, clearly indicating that the porphyrin is flattened and that π-conjugation between the porphyrin core and the *meso* pyridinium groups is increased. Therefore, the proposed structural model is in good agreement with theoretical calculations showing a dihedral angle of ~60° which induces a ~30 nm bathochromic shift in the Soret absorption band of **TMPyP^{4+}** [28]. We presume that a similar packing between **TMPyP^{4+}** and **BPh$_4^-$** takes place within previously reported nanoparticles of porphyrin without self-aggregation [20,21].

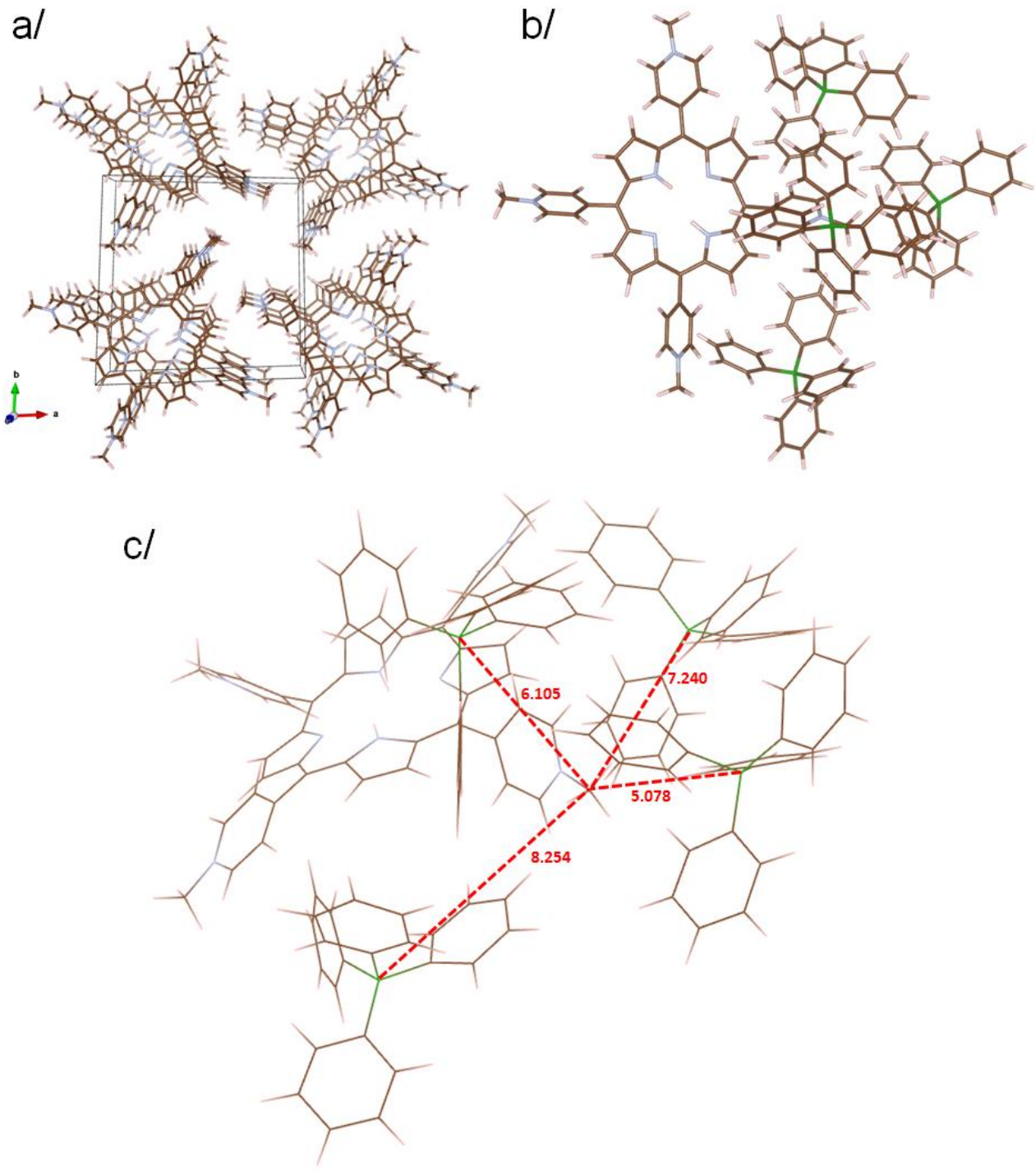

Fig. 5. a/ View of the packing of **TMPyP^{4+}** along the *c* crystallographic axis (**BPh$_4^-$** omitted for clarity). b/ Representation of the assymetric unit. c/ Representation of the coordination of the *meso* 4-N-methylpyridyl group / BPh_4^- showing the B---C(Me) distances (dashed red lines, distances in Å).

Regarding cation/anion associations, each of the positively-charged *meso* 4-N-methylpyridyl groups of **TMPyP^{4+}** was found to be surrounded by four **BPh$_4^-$** anions, according to the following layout (Figures 5b and 5c): (i) one **BPh$_4^-$**

anion is aligned with the *meso* 4-N-methylpyridyl group with a B---C(Me) distance close to 5.1 Å, (ii) two $\mathbf{BPh_4^-}$ anions are nested between two *meso* 4-N-methylpyridyl group with B---C(Me) distances between ~7.3-8.3 Å and (iii) the last $\mathbf{BPh_4^-}$ anion is located above the *meso* 4-N-methylpyridyl group (with a B---C(Me) distance ~6.1 Å). It is worth noting that the B---H(Me) and B---H(NH) distances are in line with ^{1}H-^{11}B correlations observed by solid state NMR spectroscopy (Figure 3), because the shortest B---H(Me) and B---H(NH) are ~4.3 and 7.9 Å, respectively. This explains why a longer contact time was needed in $^{1}H \rightarrow {}^{11}B$ CPMAS to observe a cross-peak between B and N<u>H</u> signals compared to B and C<u>H</u>$_3$ signals.

CONCLUSION

In this article, we have been able to synthesize and determine the structure of porphyrin nanorods, which are formed by self-assembly of two organic ions, namely free base *meso* 5,10,15,20-tetrakis-(4-N-methylpyridinium)porphyrin cations ($\mathbf{TMPyP^{4+}}$) and tetraphenylborate anions ($\mathbf{BPh_4^-}$). The use of a combined experimental-computational approach, combining high-resolution synchrotron X-ray powder diffraction, multinuclear solid state NMR, and DFT calculations (including *ab initio* calculations of NMR parameters) was found to be critical to derive the structural model of these nano-objects. We expect similar "NMR-crystallography" types of strategies to be more commonly used in the future for the study of other porphyrin-based nano-objects.

EXPERIMENTAL PART

Materials & general methods

Free base *meso*-tetrakis(4-pyridyl)porphyrin was synthesized from pyrrole and 4-pyridylcarboxyaldehyde *via* the method of Adler et al. [29]. Alkylation of free base *meso*-tetrakis(4-pyridyl)porphyrin with iodomethane was performed *via* reported procedure to obtain $\mathbf{TMPyPI_4}$ [30]. $NaBPh_4$ was purchased from Aldrich and used as received. Samples for transmission electron microscopy (TEM) measurements were prepared by deposition of a drop of nanorod suspension in EtOH on a copper grid. TEM measurements were carried out at 100 kV using a JEOL 1200 EXII microscope. Scanning electron microscopy measurements (SEM) were conducted on a Hitachi S4800 instrument. Powdered samples were simply deposited on double face tape and then Pt-metallized by sputtering under vacuum. The surface morphology of the samples was characterized by Atomic Force Microscopy (AFM) (NanoScope V, Bruker) in tapping mode using a commercial silicon probe (resonant frequency ~300 kHz and spring constant ~20 N/m) in ambient conditions. UV-visible absorption spectra were recorded on a PerkinElmer Lambda 35 spectrophotometer in 10 mm quartz cells in water.

Preparation of porphyrin nanorods.

Stock solutions of $\mathbf{TMPyP.I_4}$ (18 mg) in water (50 mL, concentration 0.3 mM) and $\mathbf{NaBPh_4}$ (22.5 mg) in water (50 mL, concentration 1.2 mM) were first prepared. Then, four identical solutions were prepared by mixing absolute ethanol (30 mL), water (2 mL), and the stock solution of $\mathbf{NaBPh_4}$ (4 mL), and placed in a thermostated bath at 30°C for one hour. Then, the stock solution of $\mathbf{TMPyPI_4}$ (4 mL) was added in the four reaction mixtures (final concentrations of $\mathbf{TMPyPI_4}$ and $\mathbf{NaBPh_4}$ were 0.03 and 0.12 mM, respectively in EtOH/H_2O 3:1). After 24 hours of vigorous stirring at 30°C in the dark, the obtained brown solids contained in each reactor were filtered together (millipore, 022 µm pore size). Then, they were dispersed in absolute ethanol and centrifugated at 20 000 rpm for 10 minutes before removing the supernatant (this step was repeated two times). Finally, porphyrin nanofibers were filtered (millipore, 022 µm pore

size), washed with absolute ethanol and dried under vacuum. Yield: 3.7 mg. The synthesis of porphyrin nanorods was repeated several times to obtain up to ~20 mg of porphyrin nanorods.

Solid state NMR analyses.

Solid state NMR experiments were performed at 14.1 T using a VNMRS-600 MHz instrument equipped with a 1.6mm triple resonance probe, spinning at 30 to 40 kHz. ^{1}H MAS (magic angle spinning) NMR spectra were acquired spinning at 40 kHz, using a one pulse sequence with probe-background suppression by DEPTH. The ^{1}H 90° excitation pulse was set to 2.5 μs. Recycle delays between 2 and 200 s were used, depending on the sample, and 16 scans were acquired. ^{11}B MAS NMR experiments were conducted spinning at 40 kHz, using a 1.5 μs ^{11}B excitation pulse, and spinal-64 ^{1}H decoupling (100 kHz RF) during acquisition. The recycle delay was set to 12 s, and 12 scans wee acquired for each sample. Two-dimensional ^{1}H→^{11}B CPMAS experiments were performed spinning at 40 kHz, using a 2.5 μs ^{1}H excitation pulse, followed by contact times of 4 or 8 ms, and applying spinal-64 ^{1}H decoupling during acquisition. The recycle delay was set to 3.5 s, and up to 200 transients were acquired for each of the 4 (or 8) increments of the 2D. The ^{1}H→^{13}C CPMAS NMR experiments were performed spinning at 30 kHz, using a 2.5 μs ^{1}H excitation pulse, followed by a 2.5 ms contact time, and applying spinal-64 ^{1}H decoupling during acquisition. The recycle delay was set between 3 to 16 s, depending on the sample, and the number of transients acquired ranged from 20 to 3500. ^{1}H, ^{13}C and ^{11}B chemical shifts were referenced externally to adamantane (^{1}H shift at 1.8 ppm and high-frequency ^{13}C shift at 38.5 ppm), and $NaBH_4$ (^{11}B shift at -42.05ppm).

High-resolution synchrotron X-ray powder diffraction

High-resolution synchrotron X-ray powder diffraction (S-XRPD) data were collected at the Soleil synchrotron Soleil (Saint-Aubin, France) on the CRISTAL beamline, using the two 2-circle diffractometer in parallel beam Debye−Scherrer geometry with the 21 Si(111) crystal multianalyzer stage [31]. The sample was previously loaded into a 0.7 mm glass capillary, and measurements were performed at 125 K and at room temperature using a wavelength λ = 0.726466 Å from 0° to 40°, with a 0.002° step. Examination of the XRPD patterns using the FoX (Free Objects for Crystallography) software [32] showed that the nanorods crystallize in the triclinic crystal system, space group P1, with the following unit cell parameters: a~16.611 Å, b~16.63633 Å, c~11.80891 Å, α~110.79°, β~110.67°, γ~82.86°. Starting from the determined parameters, the unit cell parameters were determined for both temperatures using Lebail method using the Jana2006 software package [33]. The structural model was obtained by using FoX software considering a **TMPyP^{4+}/BPh$_4^-$** 1:4 ratio. The initial structural model obtained by FoX was then optimized by DFT calculations.

DFT calculations.

The unit cell parameters were set to the X-ray diffraction parameters and kept fixed during geometry optimizations to ensure consistency between experimental and optimized structures. Protons were initially positioned to be consistent with the expected structure of the system and all atomic positions were then relaxed with the VASP (Vienna Ab-initio Simulation Package) code [34] based on the Kohn-Sham Density Functional Theory (DFT) and using a plane-wave pseudopotential approach. The NMR parameters were then calculated within Kohn-Sham DFT using the QUANTUM-ESPRESSO code [35-37], keeping the atomic positions equal to the values previously calculated with VASP. The PBE generalized gradient approximation [38] was used and the valence electrons were described by norm conserving pseudopotentials [39] in the Kleinman Bylander form [40]. The shielding tensor was computed using the Gauge Including Projector Augmented Wave (GIPAW) approach [41], which enables the reproduction of the results of a fully

converged all electron calculation [42]. The isotropic chemical shift δ_{iso} is defined as $\delta_{iso} = -[\sigma - \sigma_{ref}]$ where σ is the isotropic shielding and σ_{ref} is the isotropic shielding of the same nucleus in a reference system. For ^{1}H, ^{13}C and ^{11}B, σ_{ref} was fixed so that the average sum of experimental and calculated shifts of a series of reference compounds coincide [43]. The principal components V_{xx}, V_{yy}, and V_{zz} of the electric field gradient (EFG) tensor defined as $|V_{zz}| \geq |V_{xx}| \geq |V_{yy}|$ are obtained by diagonalisation of the calculated tensor. The quadrupolar interaction can then be characterized by the quadrupolar coupling constant C_Q and the asymmetry parameter η_Q, which are defined as : $C_Q = eQV_{zz}/h$ and $\eta_Q = (V_{yy} - V_{xx})/V_{zz}$ (e is the proton charge, h Planck's constant and Q the quadrupole moment of the considered nucleus). The Q values reported by Pyykkö were used in the calculations for ^{11}B [44].

Acknowledgements

The synchrotron powder X-ray diffraction data was recorded on the CRISTAL beamline at Soleil at Gif-sur Yvette, France (proposal #20140477). NMR spectroscopic calculations were performed using HPC resources from GENCI-IDRIS (Grant 097535). Financial support from the University of Montpellier is greatly aknowledged.

Supporting information

Figures S1-S2 and Tables S1-S3 are given in the supplementary materials. This material is available free of charge via the Internet at http://www.worldscinet.com/jpp/jpp.shtml.crystallographic data have been deposited at the Cambridge Crystallographic Data Centre (CCDC) under number CCDC-1951234. Copies can be obtained on request, free of charge, via http://www/ccdc.cam..ac;uk/data\request/cif or from the Cambridge Crystallographic Data Centre, 12 Union Road, Cambridge CB2 1EZ, UK (fax +441223-336-033 or email: deposit@ccdc.cam.ac.uk).

REFERENCES

1. Frigaard, NU, Chew AGM, Li H, Maresca JA and Bryant DA, *Photosynth. Res.* 2003; **78** 93–117.
2. Montano, GA, Bowen BP, LaBelle JT, Woodbury NW, Pizziconi VB and Blankenship R,. *Biophys. J.* 2003; **85**, 2560–2565.
3. Wagner RW and Lindsey JS, *J. Am. Chem. Soc.* 1994; **116**, 9759-9760.
4. Senge MO, Fazekas, M, Notaras EGA, Blau WJ, Zawadzka M, Locos OB and Ni Mhuircheartaigh EM, *Adv. Mater.* 2007; **19**, 2737–2774.
5. Walter MG, Rudine AB and Wamser CC, *J. Porphyrins Phthalocyanines* 2010; **14**, 759-792.
6. Fukuzumi S and Ohkubo K, *J.Mater.Chem.* 2012; **22**, 4575-458.
7. Cen TY, Whang SP, Zhang Z, Wu J and Li S, *J. Porphyrins Phthalocyanines* 2018; **22**, 726-738.
8. Gong X, Milic T, Xu C, Batteas JD and Drain CM, *J. Am. Chem. Soc.* 2002; **124**, 14290-14291.
9. Wang D, Niu, L, Qiao Z-Y, Cheng D-B, Wang J, Zhong Y, Bai F, Wang H and Fan H, *ACS Nano* 201;: **12**, 3796-3803.
10. Schwab AD, Smith DE, Rich CS, Young ER, Smith WF and de Paula JC, *J. Phys. Chem. B* 2003; **107**, 11339-11345.
11. Mongwaketsi N, Mayedwa N, Matinise N, Kaviyarasu K, Sparrow R and Maaza M, *J. Porphyrins Phthtalocyanines* 2018; **22**, 303-317.
12. Wang Z, Ho KJ, Medforth CJ and Shelnutt JA, *Adv. Mater.* 2006; **18**, 2557-2560.
13. Wang Z, Medforth CJ and Shelnutt JA, *J. Am. Chem. Soc.* 2004; **126**, 1954-15955.
14. Medforth CJ, Wang Z, Martin KE, Song Y, Jacobsen JL and Shelnutt JA, *Chem. Commun.* 2009; 7261-7277

15. Maiti NC, Mazumdar S and Periasamy N, *J. Phys. Chem. B* 1998; **102**, 1528-1538.
16. Wang L, Chen Y and Jiang J, *Nanoscale* 2014; **6**, 1871-1878.
17. Rananaware A, Bhosale RS, Ohkubo K, Patil H, Jones LA, Jasckon SL, Fukuzumi S, Bhosale SV and Bhosale SV, *J. Org. Chem.* 2015; **80**, 3832-3840.
18. Zhang N, Wang L, Wang H, Cao R, Wang J, Bai F and Fan H, *Nano Lett.* 2018: **18**, 560-566
19. Mauriello Jimenez C, Aggad D, Croissant JG, Tresfield K, Laurencin D, Berthomieu D, Cubedo N, Rossel M, Alsaiari S, Anjum DH, Sougrat R, Roldan-Gutierrez MA, Richeter S, Oliviero E, Raehm L, Charnay C, Cattoën X, Clément S, Wong Chi Man M, Maynadier M, Chaleix V, Sol V, Garcia M, Gary-Bobo M, Khashab NM, Bettache N and Durand J-O, *Adv. Funct. Mat.* 2018; 1800235.
20. Ou Z-M, Yao H and Kimura K, *Chem. Lett.* 2006: **35***,* 782-783.
21. Ou Z-M, Yao H and Kimura K, *Photochem.Photobiol.A* 2007; **189**, 7-14.
22. Garcia-Sampedro A, Tabero A, Mahamed I and Acedo P, *J. Porphyrins Phthalocyanines* 2019: **23**, 11-27.
23. Cenklova V, *Photochem. Photobiol. B* 2017; **173**, 522-537.
24. Shi DF, Wheelhouse RT, Sun D and Hurley LH, *J. Med. Chem.* 2001; **44**, 4509-4523.
25. Freyer MW, Buscaglia R, Kaplan K, Cashman D and Hurley LH, Lewis EA, *Biophys. J.* 2007; **92**, 2007-2015.
26. Guo K, Pourpak A, Beetz-Rogers K, Gokhale V, Sun D and Hurley LH, *J. Am. Chem. Soc.* 2007; **129**, 10220-10228.
27. Siddiqui-Jain A, Grand CL, Bearss DJ and Hurley LH, *Proc. Natl. Acad. Sci. U. S. A.* 2002; **99**, 11593-11598.
28. Chernia Z and Gill D, *Langmuir* 1999; **15**, 1625-1633.
29. Adler AD, Longo FR, Finarelli JD, Goldmacher J, Assour J and Korsakoff L, *J. Org. Chem.*1967; **32**, 467.
30. Monteiro AR, Ramos CIV, Fateixa S, Moura NMM, Neves MGPMS and Trindade T, *ACS Omega*, 2018; **3**, 11184−11191.
31. Hodeau J-L, Bordet P, Anne M, Prat A, Fitch AN, Dooryhee E, Vaughan G and Freund AK, *Proc. SPIE* 1998; **3448**, 353−361.
32. Favre-Nicolin V and Cerny R, *J. Appl. Cryst.* 2002; **35**, 734-743.
33. Petříček V, Dušek M and Palatinus L, *Z. Kristallogr.* 2014; **229**, 345-352.
34. Kresse G and Hafner J, *Phys. Rev. B* 1994; **49**, 14251-14269.
35. Giannozzi P, Baroni S, Bonini N, Calandra M, Car R, Cavazzoni C, Ceresoli D, Chiarotti GL, Cococcioni M, Dabo I, Dal Corso A, de Gironcoli S, Fabris S, Fratesi G, Gebauer R, Gerstmann U, Gougoussis C, Kokalj A, Lazzeri M, Martin-Samos L, Marzari N, Mauri F, Mazzarello R, Paolini S, Pasquarello A, Paulatto L, Sbraccia C, Scandolo S, Sclauzero G, Seitsonen AP, Smogunov A, Umari P and Wentzcovitch RM, *J. Phys. Cond. Matt.* 2009; **21**, 395502.
36. http://www.pwscf.org.
37. Baroni S, de Gironcoli S, Dal Corso A and Giannozzi P, Rev. Mod. Phys. 2001; **73**, 515-562.
38. Perdew JP, Burke K and Ernzerhof M, *Phys. Rev. Lett.* 1996; **77**, 3865-3868.
39. Troullier N and Martins JL, *Phys. Rev. B* 1991; **43**, 1993-2006.
40. Kleinman L and Bylander D, *Phys. Rev. Lett.* 1982; **48**, 1425-1428.
41. Pickard C and Mauri F, *Phys. Rev. B* 2001; **63**, 245101.
42. Lejaeghere K, Bihlmayer G, Björkman T, Blaha P, Blügel S, Blum V, Caliste D, Castelli IE, Clark SJ, Dal Corso A, de Gironcoli S, Deutsch T, Dewhurst JK, Di Marco I, Draxl C, Dułak M, Eriksson O, Flores-Livas JA, Garrity KF, Genovese L, Giannozzi P, Giantomassi M, Goedecker S, Gonze X, Grånäs O, Gross EKU, Gulans A, Gygi F, Hamann DR, Hasnip PJ, Holzwarth NAW, Iuşan D, Jochym DB, Jollet F, Jones D, Kresse G, Koepernik K,

Küçükbenli E, Kvashnin YO, Locht ILM, Lubeck S, Marsman M, Marzari N, Nitzsche U, Nordström L, Ozaki T, Paulatto L, Pickard CJ, Poelmans W, Probert MIJ, Refson K, Richter M, Rignanese GM, Saha S, Scheffler M, Schlipf M, Schwarz K, Sharma S, Tavazza F, Thunström P, Tkatchenko A, Torrent M, Vanderbilt D, van Setten MJ, van Speybroeck V, Wills JM, Yates JR, Zhang GU and Cottenier S, *Science* 2016; **351**, 1415-1423.

43. Berthomieu D, Gervais C, Renaudin G, Reinholdt M, Sene S, Smith ME, Bonhomme C and Laurencin D, *Eur. J. Inorg. Chem.* 2015; 1182-1191.
44. Pyykkö P, *Mol. Phys.* 2008; **106**, 1965-1974.

Synthesis, characterization and modeling of self-assembled porphyrin nanorods

Danielle Laurencin, Pascal G. Yot, Christel Gervais, Yannick Guari, Sébastien Clément, Erik Elkaim, Matthieu Paillet, Didier Cot, Sébastien Richeter

Porphyrin nanorods prepared by "ion-association" method were characterized at the molecular level by combining different techniques including multinuclear solid state NMR spectroscopy, synchrotron X-ray powder diffraction and DFT calculations.

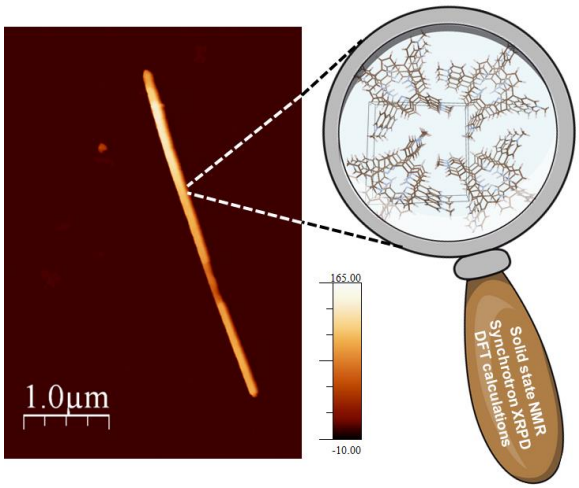

Synthesis, characterization and modeling of self-assembled porphyrin nanorods

Danielle Laurencin[a], Pascal Yot[a], Christel Gervais[b], Yannick Guari[a], Sébastien Clément[a], Erik Elkaim[c], Matthieu Paillet[d], Didier Cot[e] and Sébastien Richeter*[a]

a Institut Charles Gerhardt de Montpellier, ICGM, UMR 5253, CNRS UM ENSCM, 34095 Montpellier, France
b Laboratoire de Chimie de la Matière Condensée de Paris, LCMCP, UMR 7574, Sorbonne Université, Collège de France, 75005 Paris, France
c Synchrotron SOLEIL, L'Orme des Merisiers Saint-Aubin, BP 48, 91192 Gif-sur-Yvette, France
d Laboratoire Charles Coulomb, L2C, UMR 5221, CNRS UM, 34095 Montpellier, France
e Institut Européen des Membranes, IEM, UMR 5635, Université Montpellier, ENSCM, CNRS, 34095 Montpellier, France

SUPPORTING INFORMATION

Figure S1. 2D $^{1}H \rightarrow {}^{13}C$ CPMAS spectrum of the nanorods.

Figure S2. Structure-independent refinement of the unit-cell of the diffraction pattern obtained for the nanorods at *room temperature*.

Table S1. Unit cell parameters, unit cell volume, space group and factors of agreement obtained for the nanorods, for the two considered temperatures.

Table S2. GIPAW-DFT calculated δ_{iso} (in ppm), C_Q (in MHz) and η NMR parameters for ^{11}B, ^{13}C and ^{1}H, in the "Rel-H" model of the nanorods.

Table S3. GIPAW-DFT calculated δ_{iso} (in ppm), C_Q (in MHz) and η NMR parameters for ^{11}B, ^{13}C and ^{1}H, in the "Rel-tot" model of the nanorods.

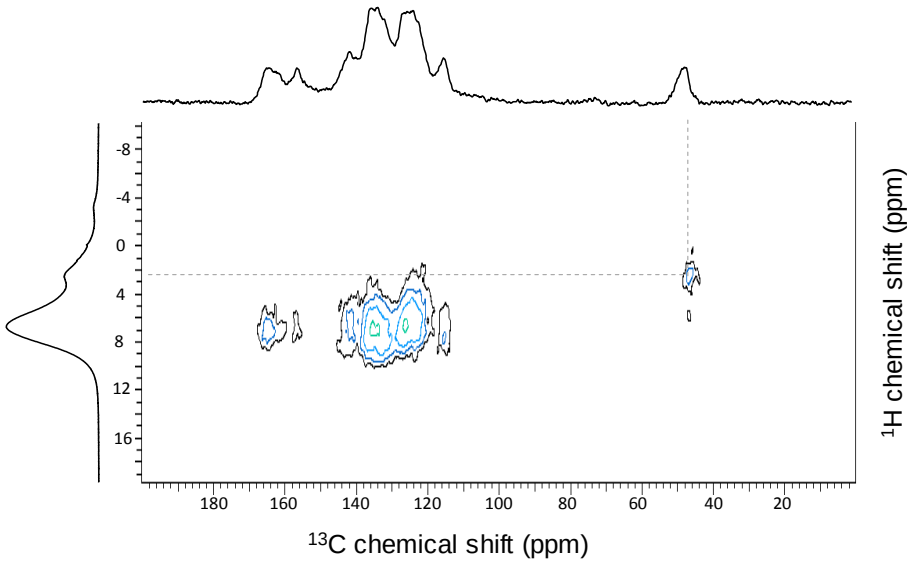

Figure S1. 2D ^{1}H→^{13}C CPMAS spectrum of the nanorods, confirming the assignment of the ^{1}H resonance centered at ~2 ppm to methyl group protons. The spectrum was recorded at 14.1 T, spinning at 30 kHz, with a contact time of 2 ms, and spinal-64 ^{1}H decoupling during acquisition. The projections shown along both axes correspond to the 1D ^{1}H MAS and ^{13}C CPMAS NMR spectra.

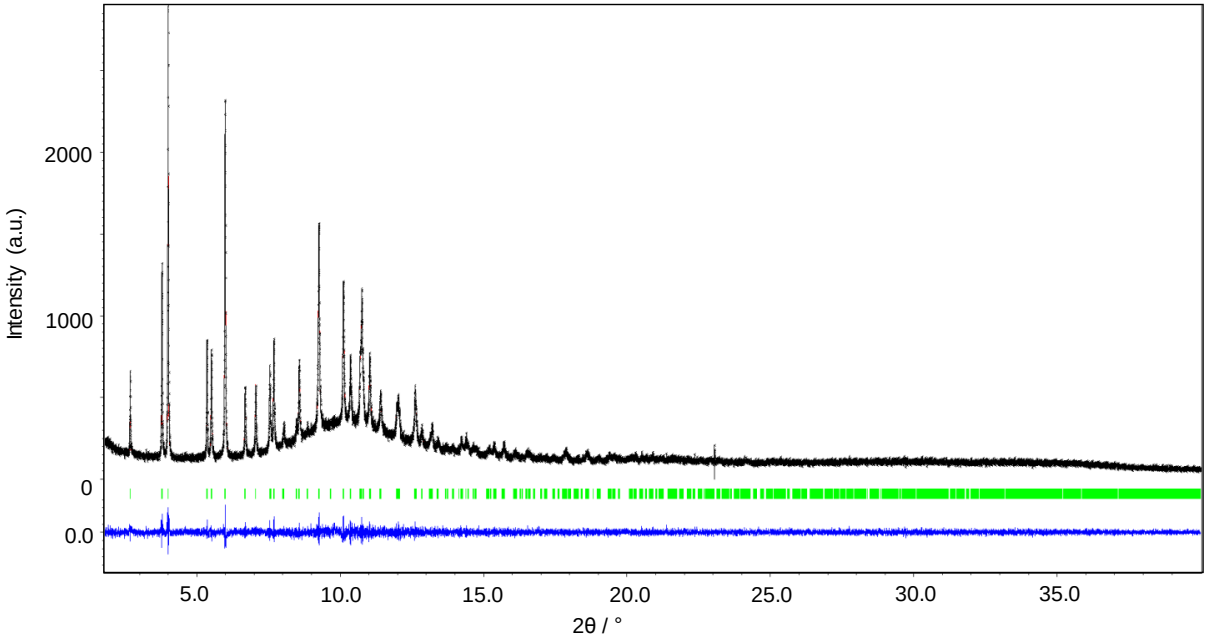

Figure S2. Structure-independent refinement of the unit-cell of the diffraction pattern obtained for the nanorods at *room temperature*. Observed (black line) and calculated (red line) X-ray powder diffraction profile for the LeBail refinement. The bottom curve (in blue) is the difference plot on the same scale intensity and the bars (in green) are the calculated angles for the Bragg peaks in 2θ.

Table S1. Unit cell parameters, unit cell volume, space group and factors of agreement obtained for the nanorods, for the two considered temperatures.

Temperature	**125 K**	**Room temperature**
Formula	$B_4\ C_{140}\ H_{118}\ N_8$	
Molar mass (g.mol^{-1})	1955.78	
Space Group	P1 (No. 1)	
Z	1	
a (Å)	16.563(2)	16.611(1)
b (Å)	16.5729(6)	16.636(2)
c (Å)	11.6236(2)	11.8089(3)
α (°)	110.636(3)	110.79(1)
β (°)	110.54(2)	110.672(4)
γ (°)	82.95(1)	82.860(8)
Vol. (Å^3)	2796.2(1)	2858.0(1)
density	1.1615	1.1378
GoF	1.04	0.91
Rp	2.85	5.53
wRp	3.75	7.17

Table S2. GIPAW-DFT calculated δ_{iso} (in ppm), C_Q (in MHz) and η NMR parameters for ^{11}B, ^{13}C and ^{1}H, in the "Rel-H" model of the nanorods (in which only H atom positions are relaxed).

	δ_{iso}	C_Q	η
B1	-13.9	-0.28	0.14
B2	-8.6	0.26	0.67
B3	-9.8	0.21	0.93
B4	-5.0	-0.13	0.35

	δ_{iso}		δ_{iso}
C1	175.5	**H1**	6.6
C2	152.1	**H2**	4.7
C3	134.0	**H3**	5.7
C4	124.6	**H4**	6.6
C5	133.2	**H5**	5.4
C6	141.1	**H6**	8.0
C7	177.4	**H7**	9.3
C8	144.2	**H8**	7.9
C9	130.2	**H9**	7.1
C10	128.8	**H10**	8.3
C11	171.8	**H11**	6.6
C12	150.9	**H12**	6.0
C13	137.5	**H13**	8.0
C14	124.5	**H14**	7.1
C15	173.2	**H15**	6.4
C16	143.9	**H16**	4.9
C17	134.6	**H17**	4.4
C18	127.4	**H18**	8.1
C19	132.8	**H19**	13.2
C20	140.9	**H20**	7.0
C21	144.0	**H21**	4.6
C22	126.6	**H22**	5.5
C23	136.2	**H23**	10.2
C24	126.1	**H24**	6.7
C25	157.6	**H25**	7.2
C26	109.4	**H26**	6.5
C27	120.4	**H27**	6.0
C28	136.7	**H28**	9.0
C29	161.0	**H29**	8.4
C30	132.0	**H30**	7.1
C31	152.4	**H31**	7.2
C32	167.1	**H32**	7.5
C33	165.3	**H33**	6.2
C34	128.2	**H34**	7.7
C35	131.2	**H35**	3.5

C36	167.9	**H36**	8.8
C37	140.1	**H37**	7.7
C38	117.6	**H38**	5.6
C39	126.9	**H39**	4.3
C40	145.8	**H40**	8.8
C41	126.7	**H41**	7.4
C42	161.0	**H42**	9.0
C43	138.1	**H43**	8.3
C44	148.8	**H44**	9.6
C45	134.3	**H45**	6.9
C46	148.3	**H46**	9.8
C47	141.1	**H47**	7.7
C48	137.8	**H48**	7.4
C49	164.7	**H49**	7.4
C50	145.0	**H50**	5.5
C51	145.3	**H51**	9.8
C52	153.9	**H52**	7.2
C53	130.0	**H53**	5.1
C54	153.8	**H54**	7.4
C55	144.2	**H55**	6.9
C56	133.6	**H56**	5.6
C57	147.4	**H57**	7.5
C58	147.4	**H58**	10.1
C59	143.9	**H59**	7.6
C60	174.1	**H60**	6.3
C61	126.6	**H61**	4.7
C62	137.0	**H62**	5.4
C63	159.2	**H63**	1.4
C64	150.4	**H64**	4.8
C65	41.4	**H65**	2.7
C66	53.1	**H66**	2.6
C67	42.4	**H67**	2.0
C68	44.3	**H68**	7.2
C69	168.8	**H69**	2.5
C70	150.0	**H70**	2.5
C71	127.6	**H71**	2.0
C72	126.6	**H72**	6.5
C73	130.3	**H73**	10.0
C74	142.1	**H74**	3.2
C75	177.3	**H75**	1.7
C76	137.5	**H76**	4.2
C77	127.1	**H77**	5.8
C78	130.7	**H78**	10.1
C79	181.3	**H79**	6.0
C80	139.8	**H80**	4.1
C81	156.9	**H81**	4.1

C82	119.8	**H82**	5.6
C83	181.0	**H83**	7.1
C84	141.0	**H84**	9.6
C85	130.2	**H85**	8.7
C86	124.3	**H86**	9.7
C87	134.1	**H87**	3.9
C88	139.3	**H88**	4.9
C89	146.7	**H89**	6.2
C90	134.6	**H90**	4.8
C91	142.5	**H91**	6.8
C92	126.8	**H92**	5.9
C93	196.0	**H93**	7.7
C94	146.0	**H94**	6.4
C95	128.3	**H95**	4.9
C96	131.8	**H96**	6.6
C97	129.0	**H97**	6.3
C98	132.3	**H98**	7.1
C99	177.6	**H99**	7.4
C100	145.9	**H100**	8.0
C101	128.1	**H101**	3.9
C102	129.2	**H102**	10.5
C103	174.4	**H103**	5.8
C104	146.7	**H104**	6.8
C105	130.4	**H105**	5.5
C106	132.2	**H106**	4.4
C107	167.9	**H107**	10.0
C108	130.2	**H108**	11.0
C109	134.6	**H109**	8.4
C110	131.7	**H110**	6.8
C111	132.8	**H111**	0.9
C112	141.6	**H112**	3.2
C113	150.1	**H113**	6.3
C114	128.4	**H114**	7.9
C115	139.1	**H115**	4.5
C116	123.7	**H116**	8.0
C117	170.7	**H117**	7.6
C118	136.6	**H118**	7.0
C119	138.8		
C120	121.0		
C121	124.9		
C122	138.5		
C123	194.0		
C124	150.5		
C125	127.7		
C126	125.6		
C127	181.3		

C128	144.7
C129	127.0
C130	139.8
C131	182.2
C132	139.7
C133	129.5
C134	135.2
C135	132.7
C136	139.3
C137	140.1
C138	136.3
C139	142.0
C140	137.1

Table S3. GIPAW-DFT calculated δ_{iso} (in ppm), C_Q (in MHz) and η NMR parameters for ^{11}B, ^{13}C and ^{1}H, in the "Rel-tot" model of the nanorods (in which all atom positions are relaxed).

	δ_{iso}	C_Q	η
B1	-6.9	-0.25	0.43
B2	-9.9	0.38	0.16
B3	-6.2	0.46	0.26
B4	-8.4	0.11	0.42

	δ_{iso}		δ_{iso}
C1	165.9	**H1**	6.1
C2	140.5	**H2**	7.2
C3	128.6	**H3**	7.5
C4	126.0	**H4**	7.3
C5	126.6	**H5**	8.0
C6	141.0	**H6**	8.3
C7	173.8	**H7**	9.8
C8	143.4	**H8**	5.6
C9	129.2	**H9**	6.1
C10	124.4	**H10**	8.2
C11	168.7	**H11**	6.5
C12	141.9	**H12**	6.2
C13	130.5	**H13**	6.7
C14	123.7	**H14**	3.1
C15	165.3	**H15**	5.2
C16	138.6	**H16**	3.6
C17	126.4	**H17**	2.3
C18	127.7	**H18**	6.3
C19	128.6	**H19**	7.5
C20	134.5	**H20**	5.4
C21	143.2	**H21**	4.8
C22	123.8	**H22**	2.9
C23	141.6	**H23**	8.7
C24	129.1	**H24**	7.6
C25	140.7	**H25**	7.0
C26	130.6	**H26**	6.3
C27	133.2	**H27**	3.8
C28	137.2	**H28**	4.2
C29	154.5	**H29**	6.1
C30	143.5	**H30**	7.2
C31	141.7	**H31**	7.1
C32	163.0	**H32**	6.4
C33	160.9	**H33**	7.0
C34	139.0	**H34**	5.5
C35	139.4	**H35**	4.1

C36	156.2	**H36**	6.5
C37	142.8	**H37**	6.1
C38	128.5	**H38**	5.2
C39	138.7	**H39**	2.3
C40	136.2	**H40**	8.1
C41	120.6	**H41**	3.7
C42	163.6	**H42**	7.2
C43	139.9	**H43**	8.4
C44	142.0	**H44**	8.6
C45	137.6	**H45**	7.5
C46	145.9	**H46**	4.9
C47	120.2	**H47**	6.5
C48	155.4	**H48**	7.0
C49	148.1	**H49**	6.5
C50	137.7	**H50**	2.5
C51	138.1	**H51**	7.6
C52	147.7	**H52**	6.2
C53	124.5	**H53**	6.1
C54	161.8	**H54**	8.5
C55	133.7	**H55**	5.9
C56	141.2	**H56**	4.8
C57	141.0	**H57**	6.7
C58	144.4	**H58**	6.1
C59	122.3	**H59**	7.2
C60	159.0	**H60**	7.7
C61	139.6	**H61**	5.2
C62	133.1	**H62**	5.3
C63	148.9	**H63**	-1.9
C64	144.0	**H64**	4.5
C65	45.2	**H65**	3.8
C66	45.6	**H66**	3.3
C67	46.4	**H67**	2.2
C68	46.8	**H68**	7.5
C69	167.0	**H69**	2.5
C70	131.1	**H70**	3.0
C71	126.7	**H71**	1.6
C72	121.7	**H72**	7.0
C73	126.3	**H73**	8.6
C74	140.7	**H74**	2.3
C75	178.8	**H75**	0.4
C76	132.1	**H76**	0.4
C77	129.6	**H77**	4.4
C78	124.7	**H78**	8.3
C79	184.0	**H79**	6.2
C80	131.7	**H80**	3.6
C81	128.8	**H81**	3.5

C82	126.0	**H82**	3.6
C83	169.0	**H83**	5.7
C84	139.1	**H84**	6.1
C85	126.2	**H85**	6.2
C86	122.0	**H86**	9.0
C87	128.0	**H87**	2.2
C88	136.0	**H88**	4.6
C89	146.9	**H89**	5.0
C90	129.2	**H90**	2.0
C91	150.4	**H91**	7.3
C92	128.6	**H92**	5.3
C93	166.4	**H93**	6.2
C94	135.0	**H94**	4.6
C95	125.7	**H95**	2.3
C96	118.8	**H96**	6.0
C97	128.5	**H97**	5.4
C98	137.0	**H98**	6.3
C99	179.9	**H99**	5.9
C100	139.7	**H100**	7.4
C101	123.6	**H101**	0.7
C102	126.3	**H102**	5.6
C103	175.5	**H103**	3.8
C104	140.7	**H104**	5.1
C105	128.3	**H105**	5.9
C106	128.7	**H106**	4.5
C107	163.8	**H107**	6.8
C108	130.3	**H108**	7.7
C109	128.1	**H109**	7.6
C110	124.1	**H110**	5.8
C111	125.4	**H111**	-2.0
C112	137.8	**H112**	2.8
C113	139.9	**H113**	7.8
C114	125.1	**H114**	8.7
C115	138.2	**H115**	5.3
C116	125.0	**H116**	7.7
C117	172.6	**H117**	6.0
C118	135.7	**H118**	5.3
C119	134.1		
C120	123.5		
C121	128.0		
C122	138.3		
C123	165.9		
C124	138.2		
C125	129.4		
C126	123.4		
C127	178.2		

C128	142.6
C129	128.5
C130	127.4
C131	171.2
C132	140.1
C133	127.5
C134	124.9
C135	129.6
C136	137.6
C137	140.0
C138	125.1
C139	140.6
C140	127.3